MRI AND DIFFUSION WEIGHTED IMAGING OF GYNECOLOGICAL CANCER

Khaled Mohammed Eltaher[1], Alsideeq Alqantari Moamer Amhalhil[2*], Osama Abdullah Dawoud[3], Enas Moustafa Ibrahim[4]

Article History: **Received:** 26.06.2023 **Revised:**04.07.2023 **Accepted:** 22.07.2023

Abstract:
Recent technical advances in diffusion-weighted imaging (DWI) greatly enhanced the clinical value of magnetic resonance imaging (MRI) of the body. DWI can provide excellent tissue contrast based on molecular diffusion and may be able to demonstrate malignant tumors. Quantitative measurement of the apparent diffusion coefficient (ADC) may be valuable in distinguishing between malignant and benign lesions.

Keywords: MRI, ovarian cancer, DWI.

[1,2,3,4]Radiodiagnosis Department, Faculty of Medicine, Zagazig University, Egypt

[*]**Corresponding Author:** Alsideeq Alqantari moamer Amhalhil
*Radiodiagnosis Department, Faculty of Medicine, Zagazig University, Egypt,
Email: alsadiqamhalhil@gmail.com, Mobile: 01123362842

DOI: 10.53555/ecb/2023.12.1033

Introduction:

The main role of using MRI in assessment of ovarian masses is its capability to characterize tissues. The presence of hemorrhage, fat, mucin, fluid, and solid components in an ovarian mass can be described with the help of MRI **(1).** MRI can be used in the evaluation and in pre-operative planning in cases of advanced ovarian cancer where pelvic spread is suspected or in cases of pelvic recurrence. It is the best method for detection of infiltration to the uterus, bladder, rectum, or pelvic sidewall**.** MRI is indicated in patients who have allergy to iodinated contrast media, pregnant or in cases where the CT findings are inconclusive or negative **(2)**.

Since many benign and malignant pelvic disorders have similar imaging characteristics, characterizing an adnexal tumor can be difficult. Since it greatly affects clinical therapy, accurate differential identification of suspected pelvic masses based on imaging is essential. Radiologists may find MRI to be helpful due to its higher contrast resolution and tissue characterization. The integration of 3T magnets into routine clinical practice and the use of the Ovarian-Adnexal Reporting and Data System (O-RADS) diagnostic criteria may help radiologists become more familiar with the symptoms of ovarian cancer and other pelvic conditions that may mimic the condition, boosting their confidence in determining the location of origin and making the most probable diagnosis (**3**).

The imaging criteria for malignant ovarian tumors:

The 1ry criteria include:

- A solid or large solid area within a cystic mass.
- Wall thickness more than 3 mm.
- Septal thickness more than 3 mm and/or vegetations or nodularity.
- Necrosis.

The ancillary criteria include:

- Infiltration of pelvic organs or the sidewall.
- Peritoneal, mesenteric, or omental disease.
- Ascites.
- Lymphadenopathy **(4).**

I. Findings of Ovarian cancer on MRI:

A. Borderline and Malignant Neoplasms:

Imaging findings indicative of borderline or malignant tumors include mural nodules, papillary projections, enhancing solid tissue (except those of fatty or fibrous nature), thickened, irregular walls or septa (i.e., diameter > 3 mm and highly vascular), and necrosis. Large size and the involvement of lymph nodes or peritoneal dissemination may suggest a borderline or malignant tumor (**5**).

1. High-Grade Serous Cystadenocarcinoma (HGSC)

HGSC usually manifests as bilateral (58% of cases), predominantly cystic masses with differing amounts of solid tissue. A few of such tumors are entirely solid. The solid component often demonstrates restricted diffusion and intense enhancement on dynamic contrast enhanced images with type 3 Time Intensity Curve (TIC) (i.e., initial slope greater than myometrium and marked increase in signal intensity with a plateau or washout) (**6**). It usually presents with extraovarian disease at diagnosis, including peritoneal dissemination, pelvic organ invasion, ascites, and lymphadenopathy (**7, 8**) (**Figure 1**).

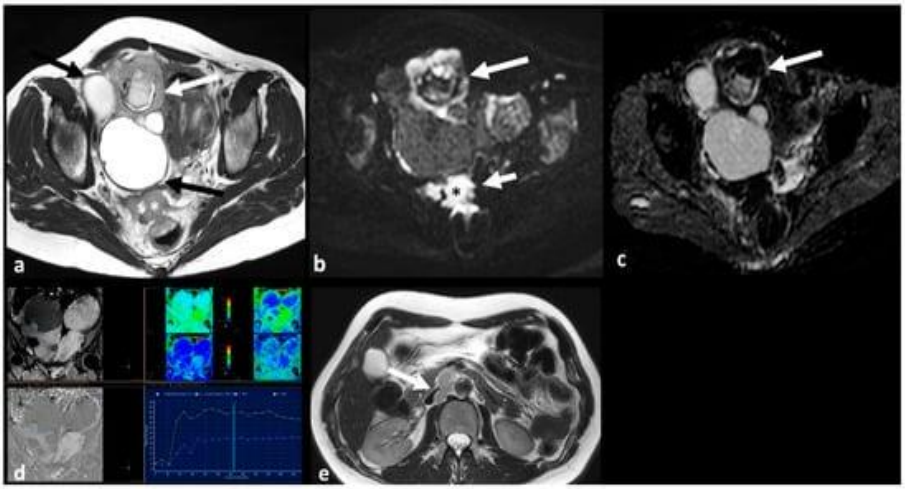

Figure (1): High grade serous cystadenocarcinoma with peritoneal and lymph node metastases. Axial T2 weighted image (**a**) shows a multiloculated right ovarian cystic mass (black arrows) with a large solid component (white arrow). The solid portion (white arrow) demonstrates high signal on axial 1200 b value DWI (**b**) and low signal on ADC map (**c**). DCE image analysis (**d**) demonstrates an intermediate-risk time

intensity curve of the solid tissue (TIC type 2, orange line: myometrium, blue line: solid tissue). Axial T2 weighted image of the upper abdomen of the same patient (**e**) shows right paraaortic lymphadenopathy (white arrow). Shown also is a large peritoneal implant in the pelvis (asterisk in (**a**); asterisk and short arrow in (**b**)) (**7**)

2. Serous Borderline Neoplasms and Low-Grade Serous Cystadenocarcinoma

Low-grade serous cystadenocarcinoma (LGSC) is uncommon, accounting for only 2.5% of ovarian malignancies. Interestingly, it can arise from and co-exist with a non-invasive serous borderline component. Compared to borderline neoplasms, women with LGSC often present at a later stage and have a poorer prognosis since LGSC is platinum-resistant (**9**) (**Figure 2**).

The solid elements enhance after intravenous contrast administration, usually with type 2 TIC on DCE images (i.e., initial slope less than myometrium, moderate increase in signal intensity with a plateau or washout). Compared to their mucinous counterparts, borderline and low-grade serous neoplasms are more often bilateral (around one-third of serous borderline tumors and the majority of LGSC) with an increased number of papillary projections (**10**) (**Figure 3**).

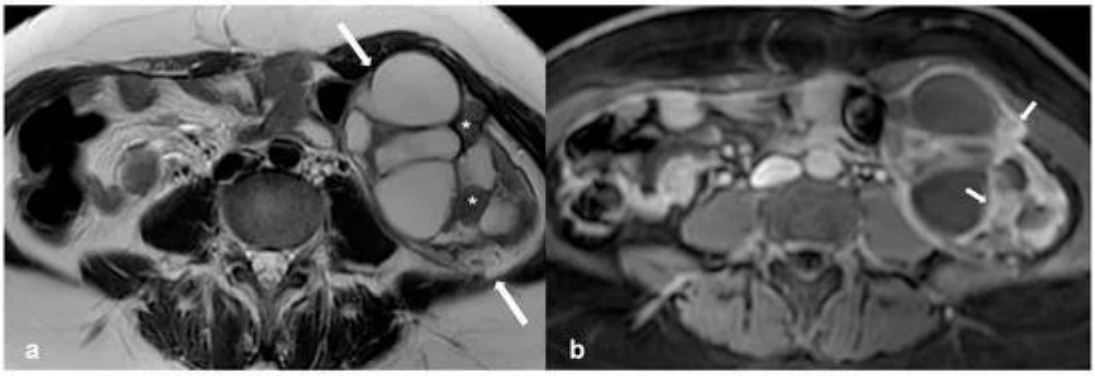

Figure (2): Low grade serous cystadenocarcinoma. Axial T2 weighted image (a) shows a multiloculated, predominantly cystic mass at the left ovary (white arrows) with solid tissue (asterisks) showing avid enhancement on the T1 weighted FS CE image ((b), white arrows) (**9**).

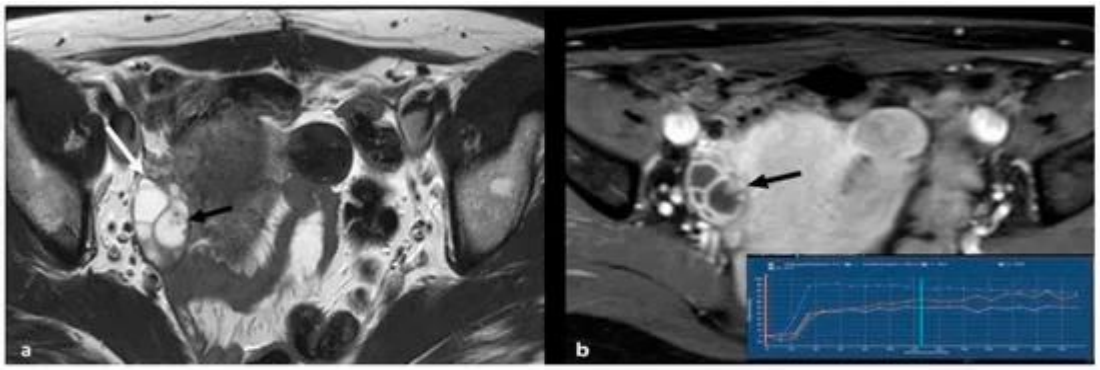

Figure (3): Serous epithelial borderline ovarian tumor. Axial T2 weighted image (a) shows a multiloculated cystic lesion at the right ovary (white arrow). A small, papillary projection (black arrow) is present, with avid enhancement on the T1 weighted FS CE image ((b), black arrow). An intermediate-risk time intensity curve (TIC type 2) was detected on DCE image analysis (inset in b, blue line: myometrium, orange/pink lines: papillary projection) (**10**).

3. Mucinous Borderline Neoplasms and Mucinous Cystadeno-carcinoma

Mucinous neoplasms are usually unilateral, confined to the ovary, and larger when diagnosed compared with serous tumors. At imaging, they appear as multilocular, predominantly cystic masses. The signal intensity of the locules may vary on MRI, because of different mucin content, the so-called stained-glass appearance (**11**) (**Figure 4**). Conversely, mucinous adenocarcinoma, which accounts for 9.4% of all invasive epithelial tumors, has the poorest prognosis of all ovarian malignancies, with low survival rates (**12**).

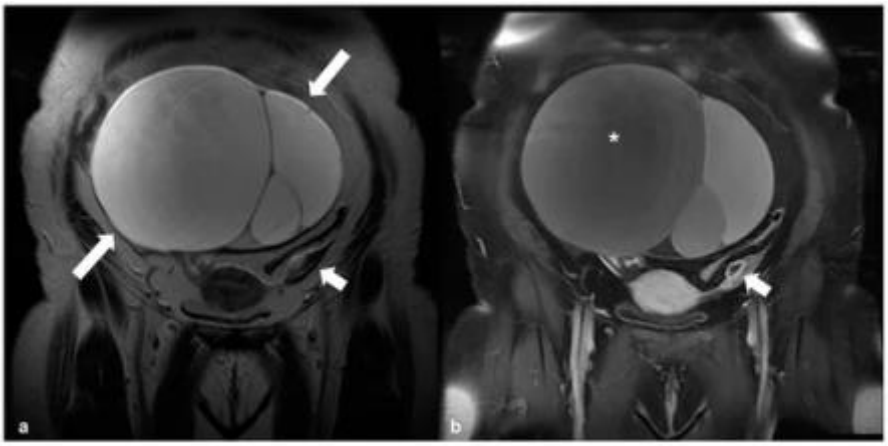

Figure (4): Mucinous cystadenoma. T2 weighted image (a) in the coronal plane, shows a large multilocular cystic mass originating from the right ovary (arrows). Corresponding T1 CE FS image (b) shows different signal intensity of various compartments (asterisk), the so-called 'stained-glass' appearance. Shown also is the normal left ovary (short arrow in (a,b)) (**11**).

4. Endometrioid Carcinoma and Clear Cell Carcinoma

Endometrioid and clear cell ovarian carcinomas are typically invasive and aggressive, although typically they are low grade neoplasm (**13**). Both commonly affect women in their fifties in the 5th decade and present at an early stage, leading to better clinical outcomes (**12**).

Imaging findings of endometrioid and clear cell carcinomas are nonspecific. High-grade endometrioid carcinoma can be indistinguishable from HGSC. Both are typically present as a mass with varying solid and cystic parts, usually more solid than serous and mucinous neoplasms, often with evidence of hemorrhage. When they develop in an endometrioma, diagnosis may be suggested by the presence of an enhancing mural nodule within an otherwise typical endometrioma (particularly with large endometriomas in women > 45 years) (**14**) (**Figure 5**).

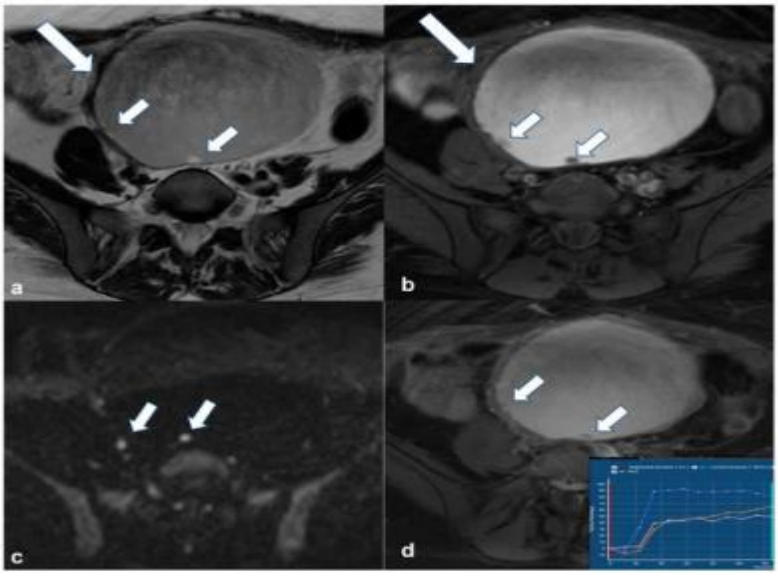

Figure (5): Endometrioid borderline ovarian tumor Axial T2 weighted image (a) shows a cystic mass (large arrow) originating from the right ovary with hemorrhagic content on corresponding axial T1 weighted FS image (b). There are small mural nodules in the right posterolateral aspect of the lesion (small arrows in a and (b)) with restricted diffusivity on corresponding axial high b value DWI image (small arrows in (c)). Note the enhancement of the nodules on the corresponding axial T1 weighted FS CE image (small arrows in (d)). DCE analysis showed a type 2 time–intensity curve (inset in (d), blue line: uterus; yellow/pink line: nodules) (**14**).

Loss of T2 shading on MRI or relatively low signal intensity may be another sign of malignancy due to dilution of hemorrhagic contents by non-hemorrhagic fluid produced by the malignant tissue (**14**).

Concurrent with ovarian tumor endometrial thickening or mass may suggest endometrioid carcinoma (**15**) (**Figure 6**). Although rare, endometrioid carcinoma is the most common malignancy arising within an endometriotic cyst, followed by clear cell carcinoma (**13**).

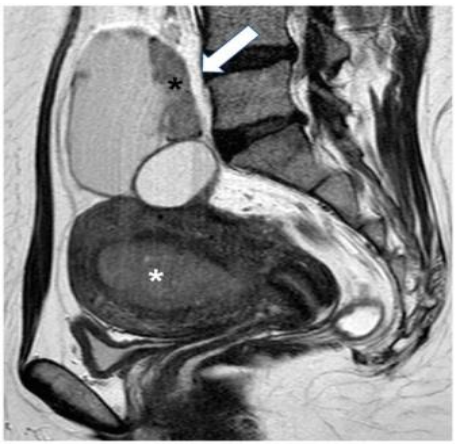

Figure (6): Synchronous ovarian and endometrial endometrioid adenocarcinoma. Sagittal T2 weighted image shows a soft-tissue mass occupying the endometrial cavity (white asterisk). Note a solid and cystic mass of the right ovary (arrow) with the solid component (black asterisk) exhibiting similar signal intensity to that of the endometrial mass (**15**).

B. Benign Neoplasms Tumors

1. Cystadenofibroma

Adenofibromas and cystadenofibromas appear as mixed solid and cystic masses, often with papillary projections. At MRI, the solid components which correspond to the fibrous stroma are characteristically quite hypointense on T2 weighted images, of lower signal intensity compared to muscle, often with internal cysts and minimal enhancement (**16**).

The low T2 signal of the septa, together with the high T2 signal of the cystic spaces give the tumor a characteristic 'black sponge' appearance (**17**) (**Figure 7**).

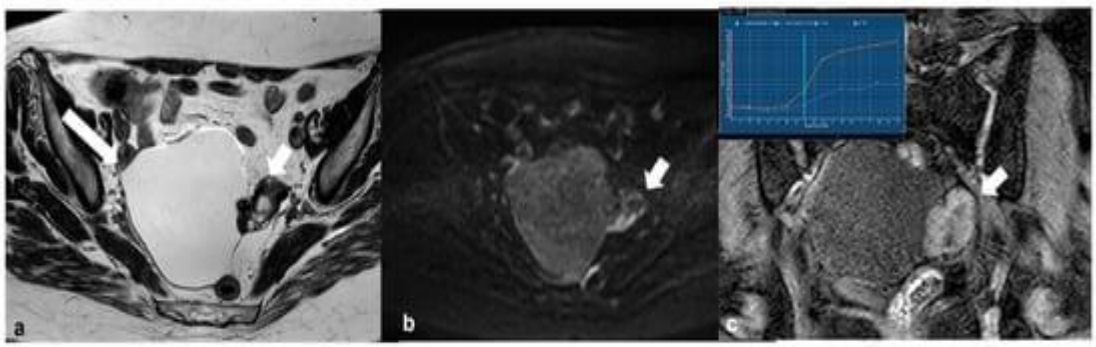

Figure (7): Cystadenofibroma. Axial T2 weighted image (a) shows a right-sided ovarian cystic mass (long arrow) with a peripheral solid component of very low signal intensity (short arrow). Corresponding axial high b value (1200) diffusion weighted image (b) shows no restricted diffusion of the solid tissue (arrow). Dynamic contrast-enhanced image (c) demonstrates avid enhancement of the solid part of the lesion (arrow) and a type 2 time–intensity curve (yellow line: uterus; blue line: lesion in inset) (**18**).

2. Fibrothecoma

On MRI, fibrothecomas present as solid ovarian masses with low T2 signal intensity relative to muscle. However, T2 signal intensity may be higher when oedema or cystic degeneration co-exist (most often in thecomas) amd low signal intensity in T1(**19**).

On DCE, most cases demonstrate minimal enhancement initially, which increases on delayed images; this perfusion pattern corresponds to TIC type 1 (i.e., mild and gradual increase in signal over time with no well-defined shoulder and no plateau) (**20**) (**Figure 8**).

Fibrothecomas are usually of larger size than Brenner tumors and calcifications are not so common, although dense calcifications may sometimes be present (**21**).

In some cases, they may be misinterpreted for a pedunculated leiomyoma, but this usually displays more intense homogeneous enhancement similar

to that of the myometrium and possibly, the bridging vessel sign (**21**) (**Figure 9**).

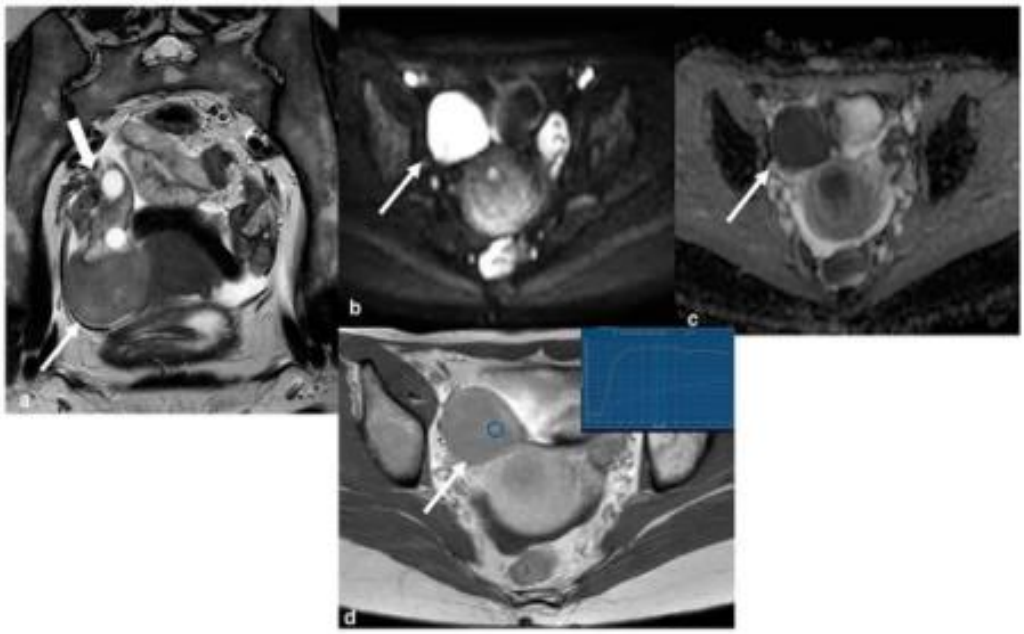

Figure (8) Cellular fibrothecoma. T2 weighted image in the axial oblique plane (a) demonstrates a rather low signal intensity lesion (long white arrow) attached to the lower pole of the right ovary (short white arrow). Corresponding axial high b value (1200) diffusion weighted image (b) and ADC map (c) show restricted diffusion of the lesion (arrow in (b,c)). The lesion shows avid contrast uptake on axial CE T1 weighted image ((d), arrow). DCE analysis of the lesion shows a type 1 time–intensity curve (inset in (d), blue line: lesion; orange line: uterus; blue circle: region of interest (ROI) within the lesion) (**20**).

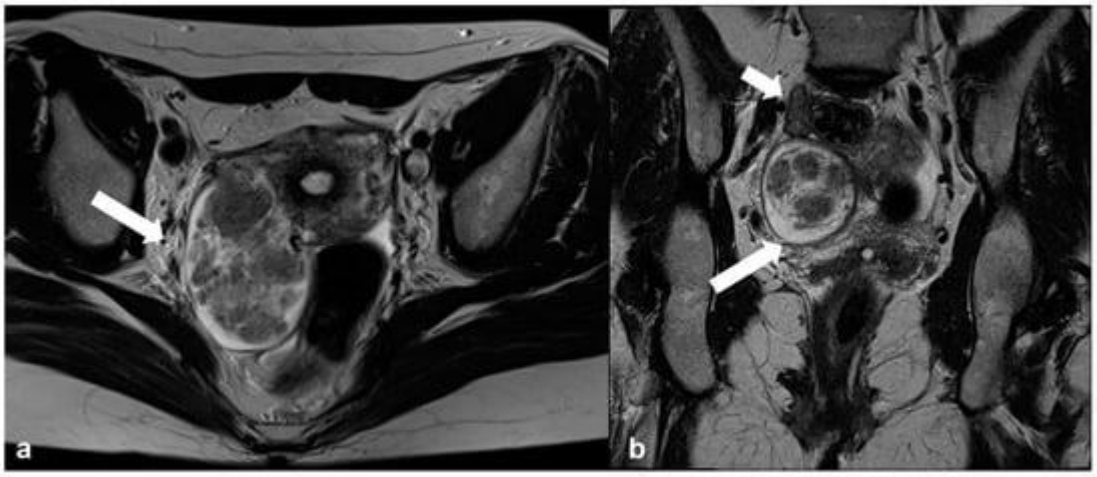

Figure (9): Degenerative pedunculated leiomyoma mimicking ovarian lesion. Axial T2 weighted image (a) shows a large inhomogeneous mass within the right broad ligament (arrow). Coronal oblique T2 weighted image (b) of the same patient shows the right ovary (short arrow) separate from the mass (long arrow) (**21**).

C. Rare Ovarian Neoplasms

1. Brenner Tumor

At imaging, brenner tumors size varies from microscopic to huge; in a series by Moon et al. including eight tumors, the mean size was reported to be 11 cm. In addition, about half of the cases demonstrated extensive amorphous punctuate calcifications. Characteristically, the solid component exhibits markedly low T2 signal intensity on MRI because of dense fibrous stroma (**22, 23**).

Brenner tumors can coexist with mucinous tumors in the same ovary. Findings suggestive of malignancy in a Brenner tumor, include large cystic parts and an inhomogeneous solid component (i.e., with mild enhancement, due to coexistence of fibrous and malignant components (**22, 24**) (**Figure 10**).

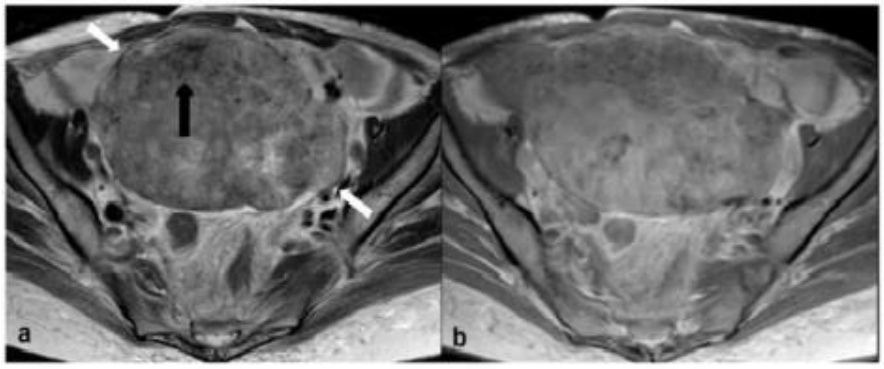

Figure (10): Malignant Brenner tumor. Axial T2 weighted image (a) shows a large, predominantly solid mass of moderately high signal intensity (white arrows) with areas of lower T2 signal (black arrow), occupying the pelvis. Axial T1 weighted CE image (b) shows mild, heterogeneous enhancement of the mass (**24**).

2. Monodermal Teratoma (Struma Ovarii)

At MRI imaging, monodermal Teratoma present with a variable mixed solid and cystic component or appear entirely solid (**25**) (**Figure 11**). They often coexist with a mature teratoma in which cases the solid component demonstrates avid enhancement. When struma ovarii is suspected, CT may be helpful in narrowing the differential diagnosis, since the solid component is often hyperattenuating on unenhanced images because of the iodine content in the thyroid tissue (**26**).

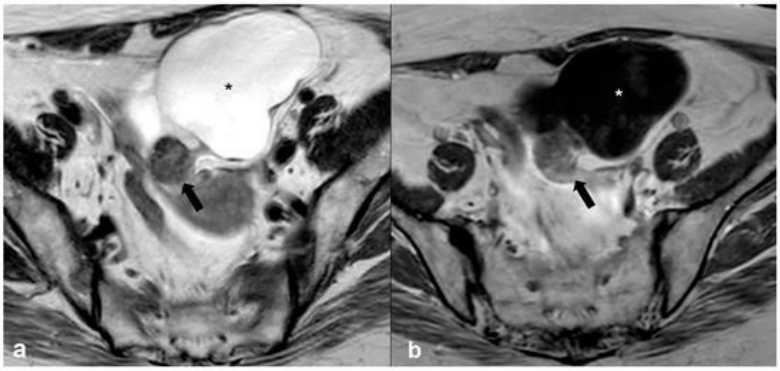

Figure (11): Struma ovarii tumor. Axial T2 weighted image (a) shows a predominantly cystic mass (asterisk) with a posteriorly located solid nodule (arrow) in the left ovary showing mild enhancement on the T1 weighted contrast-enhanced image (arrows in (b)) and corresponding to ectopic thyroid tissue (**26**).

3. Granulosa Cell Tumor

Imaging characteristics of granulosa cell tumors (GCT) vary and may overlap with those of malignant epithelial cell tumors (**27**). GCTs are usually present as large (mean size: 10–12 cm), multilocular masses with both solid and cystic components and areas of hemorrhage; they can also be purely solid or cystic. Their most characteristic appearance is that of a solid mass with a spongelike ("Swiss cheese") appearance; the tumor's cystic compartments may be hemorrhagic fluid with high T1 signal and fluid-fluid levels (**28**).

Discriminative features of GCTs from malignant epithelial cell neoplasms include absence of intracystic papillary projections, unilateral location, and confinement to the ovary. Additionally, there is a low incidence of peritoneal disease at diagnosis (**27**). Endometrial thickening or endometrioid carcinoma may co-exist due to the estrogenic effect (**29**).

4. Lymphoma

MRI features of lymphoma of the ovary include the presence of bilateral homogeneous solid masses with mild homogenous enhancement, and rather low T2 signals, due to the presence of myeloperoxidase (**30**).

Helpful signs for diagnosing ovarian lymphoma are bilaterality, bulky abdominal or pelvic nodal conglomerates, and no ascites. Other characteristic imaging signs include the presence of small peripheral cysts, which correspond to preserved ovarian follicles, and encasement of vessels and bowel by the mass without obstruction (**31**) (**Figure 12**).

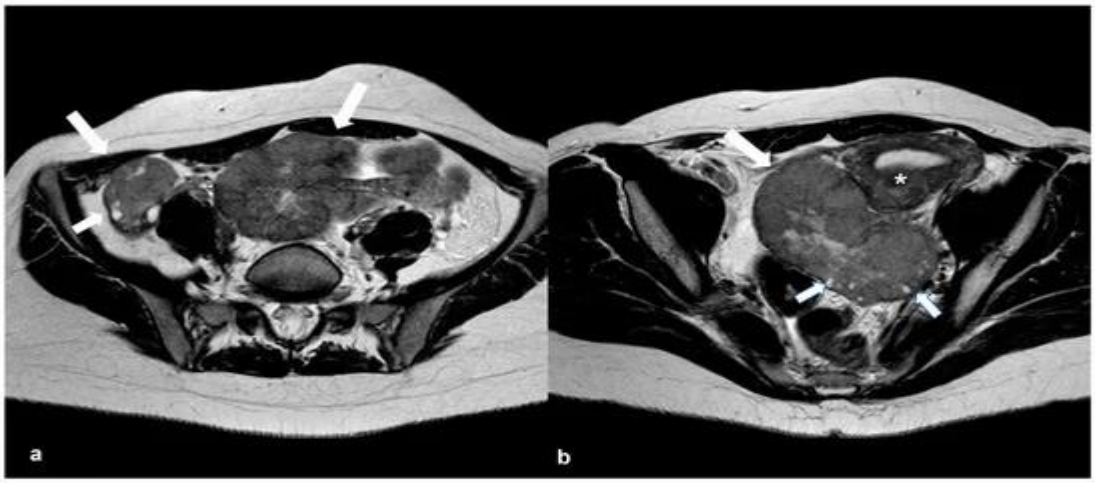

Figure (12): Primary ovarian lymphoma. Axial T2 weighted images (a,b) show bilateral ovarian enlargement (long arrows) with abnormal stromal signal intensity and peripheral displacement of the ovarian follicles (short arrows). The uterus is displaced to the left side of the pelvis by the enlarged left ovary (asterisk in (b)) (**31**).

5. Metastases

Metastases is bilateral in most cases (**32**). Imaging manifestations of metastases depend on their site of origin. Predominantly solid metastases usually originate from gastric or breast primaries, while other GI tract metastases (i.e., appendiceal, colorectal, and pancreaticobiliary) often have larger cystic components (**33**) (**Figure 13**).

At imaging, if bilateral highly vascular ovarian masses measuring less than 10 cm (or for some authors less than 15 cm) are present, metastases should be considered, especially in cases of known history of malignancy or when an extraovarian primary neoplasm with peritoneal carcinomatosis is depicted (**34**).

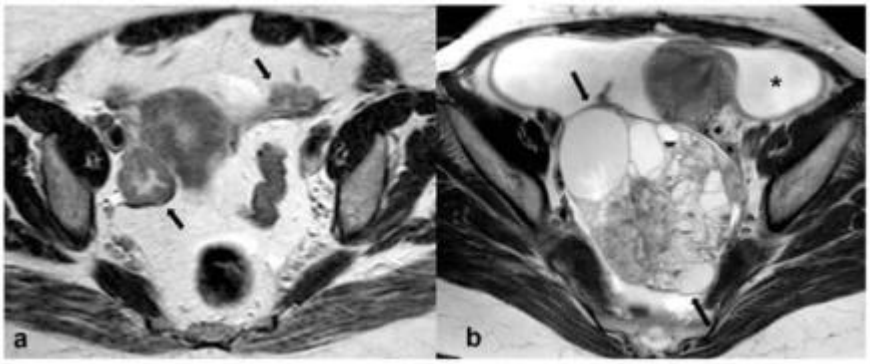

Figure (13): Metastatic ovarian cancer. Axial T2 weighted image (a) of a postmenopausal woman with primary gastric cancer. Note the presence of small predominantly solid masses in both ovaries (black arrows). Axial T2 weighted image (b) of a premenopausal woman shows a large, mixed cystic, and solid mass in the right adnexa (black arrows) originating from a colon primary. Shown also is a large amount of ascites (asterisk) (**33**).

Imaging signs supporting the diagnosis of mucinous ovarian metastasis over primary borderline or malignant mucinous tumor include (**a**) size < 10 cm (or for some authors <15 cm), (**b**) bilateral involvement, and (c) peritoneal dissemination (**35**).

A helpful sign in distinguishing primary borderline and malignant serous tumors from metastases (since they may both present as bilateral tumors with peritoneal spread), is the presence of papillary projections in the former. An imaging feature indicative of ovarian metastases from colorectal tumors is the 'mille-feuille sign' which consists of fine, alternating layers of tumor cells and necrosis with a width/length of ≥10/20 mm within the metastatic tumor (**36**).

Krukenberg Tumors

Approximately 10% of ovarian tumors are metastatic masses, almost 50% of which are Krukenberg tumors. Nearly 80% of Krukenberg tumors are bilateral (**23**) (**Figure 14**) metastatic tumor which contain well defined histological

chracterstics that is mucin secretory cells (signet ring cells) (**37)**

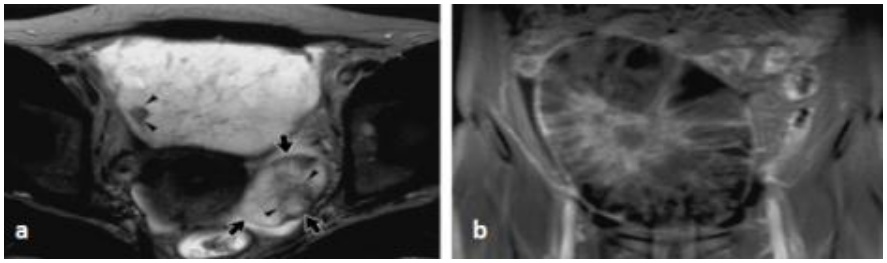

Figure (14): Bilateral metastasis (Krukenberg tumors) from gastric carcinoma in a 38-year-old woman. (a) Axial T2-WI shows bilateral cystic masses with hypointense solid portions (arrowheads). The left-sided mass (arrows) is much smaller than the right-sided mass. (b) Gd fat-suppressed T1-WI shows the mass with marked enhancement of the septa and solid components (**23**).

However, on MRI, the solid components appear to be T1 and T2 hypointense because of dense stromal reaction, and they show corresponding diffusion restriction and enhancement on contrast-enhanced sequences. T2 hyperintensity is seen in the cystic areas, representing mucin that does not enhance (**Figure 15**). Hypointense T2 solid components in an ovarian mass are characteristic of Krukenberg tumors, particularly if the tumors are bilateral with uniform cystic locules, have sharp margins, and have an oval configuration (**35**).

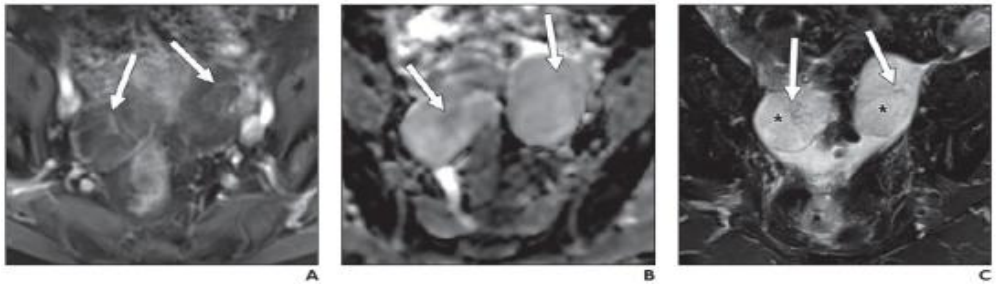

Figure (15): 42-year-old woman with cecal adenocarcinoma who presented with abdominal pain and had MRI features of Krukenberg tumors. **A**, Axial contrast-enhanced 3D fat-suppressed T1-weighted gradient-echo MRI sequence shows bilateral ovarian masses. Both masses have thick internal septations that enhance (arrows). **B**, Axial apparent diffusion coefficient sequence shows diffusion restriction corresponding to enhanced internal septations (arrows) in A. **C**, T2-weighted fat-suppressed MRI sequence highlights high signal from internal mucinous products (asterisks). Note that enhancing septations are T2 hypointense (arrows) (**35**).

D. Adolescence-Germ Cell Tumors:

Germ cell tumors represent the second largest category of ovarian neoplasms in the general population; however, they are the most frequently occurring subtype in adolescents and young adults (**38**).

1. Mature Cystic Teratoma (Dermoid)

Imaging characteristics of a mature teratoma include presence of a cystic, fat-containing mass usually with solid components (i.e., dermoid plug or Rokitansky nodule) (**5**).

At MRI, detection of fatty elements (i.e., high T1 and T2 signal and suppression of signal on fat-suppressed images) is virtually pathognomonic for teratoma. T1-weighted images with saturation of fat are the key sequence for discriminating between fat and hemorrhage (which remains T1 hyperintense). The fat-containing mass shows chemical shift artifact in a significant number of cases (62–87%) (**39**) (**Figure 16**). Moreover, DWI may be useful since almost all mature cystic teratomas, even the lipid poor, are known to have a keratinoid component which shows restricted diffusion (**40**).

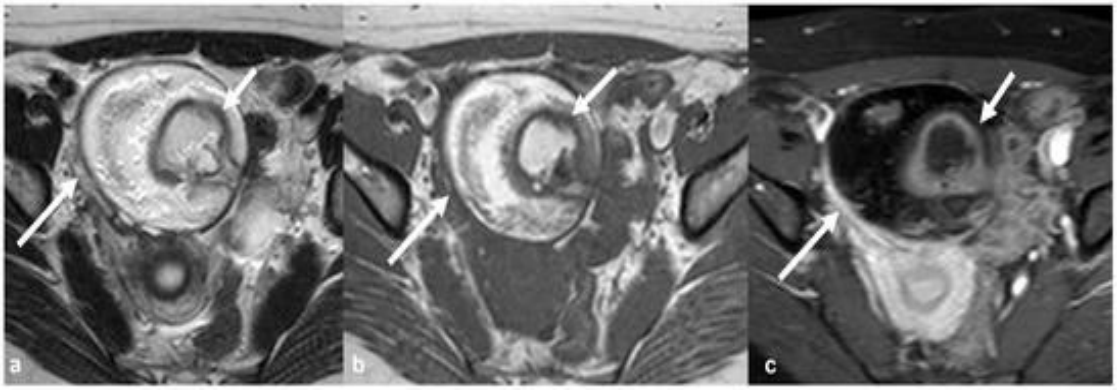

Figure (16): Mature teratoma. Axial T2 weighted image (a) shows a large, high signal intensity mass (long white arrow) in the right side of the pelvis. The mass demonstrates high signal intensity on corresponding axial T1 weighted image (b) and significant signal drop on T1 weighted FS CE image (c), typical of fatty content (long white arrow). Shown also is the typical fat-containing intra-tumoral Rokitansky nodule (short arrow in (a) and (b)) with peripheral contrast enhancement (short arrow in (c)) (**41**).

2. Immature Teratoma

At MRI, in contrast to benign mature teratomas, it tends to be unilateral and larger, more heterogeneous, with more solid elements which enhance, only small, scattered foci of fat and cystic components with usually simple fluid content. In addition, the calcification pattern seems to differ, since calcifications in immature teratoma are irregular and multiple while in mature tumors they are coarsened or toothlike (**42, 43**) (**Figure 17**).

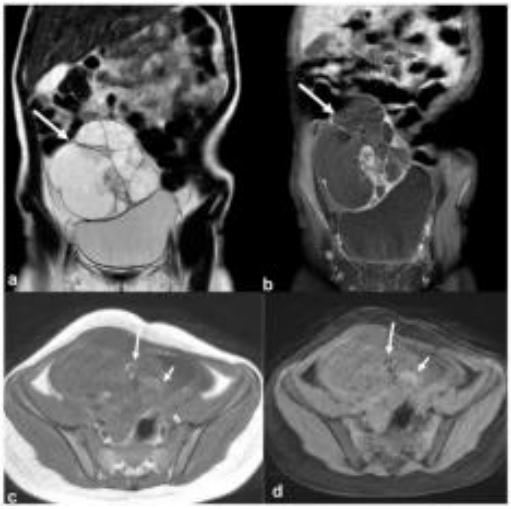

Figure (17): Immature teratoma in a 7-year-old girl. Coronal T2 weighted image (a) shows a large cystic right-sided pelvic mass (white arrow) with internal septations and smaller solid components which are enhanced on the T1 weighted FS CE image ((b), white arrow). Axial T1 weighted image (c) shows tiny foci of high signal intensity (long arrow) with signal loss on the T1 weighted FS image ((d), long arrow). Note also a few hemorrhagic foci with high T1 signal intensity on both T1 weighted images (short arrows in (c,d)) (**42**).

3. Dysgerminoma

Unlike immature teratoma, dysgerminoma may involve both ovaries in a small number of cases (10–15%) and may occasionally spread to the retroperitoneal lymph nodes (**44**).

Dysgerminoma is typically seen as a large, lobulated predominantly solid mass with internal fibrovascular septa. Because of their fibrous nature, the septa demonstrate low T2 signal intensity and intense, homogenous enhancement (**45**). Necrosis, hemorrhage, or speckled calcifications are less frequently seen within the tumor (**Figure 18**). In contrast to other fibrous ovarian tumors (i.e., Brenner tumor and fibroma/fibrothecoma), the T2 signal intensity of fibrous tissue in dysgerminomas is not lower but slightly hyperintense to muscle (**46**).

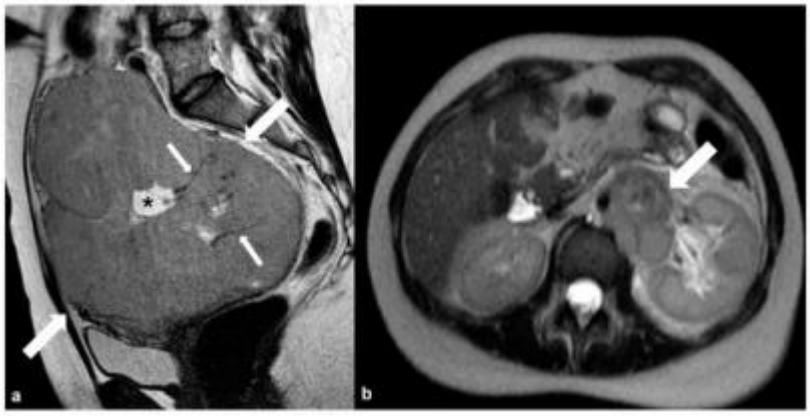

Figure (18): Dygerminoma. Axial T2 weighted image (a) shows a predominantly solid ovarian mass (large arrows) with thin low signal intensity internal septa (thin arrows) and cystic/necrotic area (asterisk). T2 weighted image (b) of the same patient at the level of the renal hilum shows multiple enlarged left paraaortic lymph nodes (arrow) (**45**).

Findings of Uterine Tumor on MRI:

1. Endometrial carcinoma

MRI: has an important role in the preoperative evaluation and surgical planning by accurately calculating the depth of myometrial invasion, cervical stromal invasion, lymph node involvement, and metastatic spread. MRI can also give additional useful information such as uterine size, tumor volume, and ascites, and can reveal adnexal abnormalities. **(47).**

Endometrial carcinoma appear isointense to the normal endometrium on unenhanced T1-weighted images. After IV contrast administration, the healthy inner myometrium enhances earlier than the outer myometrium **(48).**

Hemorrhage in the endometrial cavity can also appear of low signal intensity on T2 but become hyper intense on pre contrast T1-weighted images. The inner myometrium or junctional zone compared to tumors is hypointense on T2-weighted images. In old postmenopausal women the junctional zone is not well seen, because of this limiting factor, contrast-enhanced images have been found to be more helpful because after injection of contrast the tumor enhances less than the normal myometrium and is relatively hypointense **(49).**

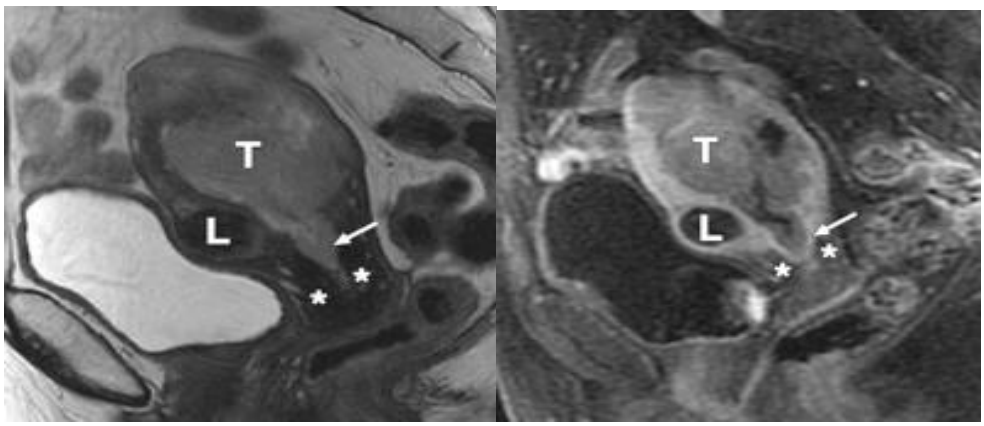

A **B**

Figure (19):: Stage IIA endometrial carcinoma in 78-year-old woman. (A) Sagittal T2-weighted image (B) fast spin-echo and gadolinium-enhanced fat-suppressed T1-weighted. MR images show endometrial carcinoma (T) with deep myometrial invasion and tumor extension into cervical canal (arrow in A). Note preservation of low-signal-intensity cervical stroma (asterisks). Normal enhancement of cervical mucosa (arrow in B) on enhanced images excludes cervical stroma invasion. Incidental presence of uterine leiomyoma (L) is noted **(50).**

2. Uterine Sarcoma

MR imaging findings are different and involve a lobulated mass of high signal intensity on T2-weighted images, a sharply marginated mass of low signal intensity that closely similar to fibroid, or a mass with localized infiltrative margins. Signal intensity is not a sure sign of malignancy. Detection of scattered dots of hemorrhage or

necrosis can serve as a clue for diagnosis of leiomyosarcoma such findings indicate coagulative necrosis, which would raise suspicion for leiomyosarcoma. At MR imaging, such necrotic areas are appear as areas of slightly high signal intensity on T1W images and heterogeneous areas on T2W images **(51).**

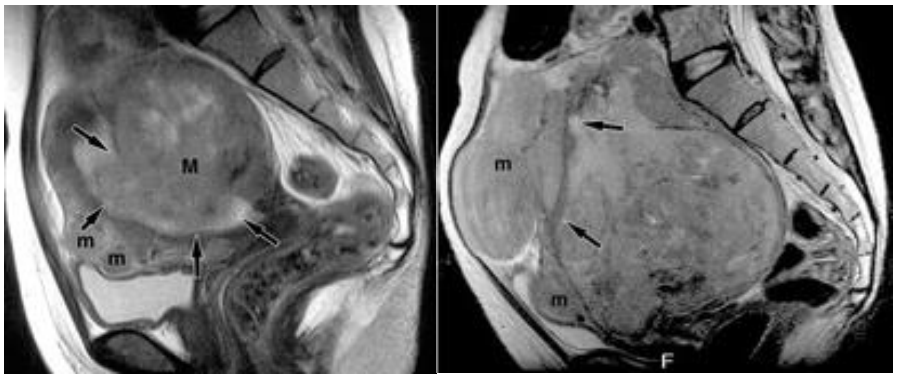

Figure (20): Leiomyosarcoma in a 44-year-old woman. (a) Sagittal T2-weighted image shows a tumor (M) with slightly high signal intensity and irregular margins. The tumor protrudes from the posterior myometrium into the endometrial cavity (arrows). Small leiomyomas (m) with clear margins are present in the anterior wall. (b) Sagittal T2-weighted image, obtained 3 months later after the patient experienced rapidly progressing abdominal fullness, shows an irregularly shaped uterus that has clearly increased in size. The tumor occupies the endometrial cavity (arrows). The nodules (m) in the anterior wall also demonstrate remarkable increase in size **(51).**

3. Uterine Choriocarcinoma

Hemorrhage on T1 is seen as hyperintense areas,
On **T1+(Gd):** heterogeneous patterns of contrast enhancement have been reported (**52**). Signal voids foci which are seen on both T1- and T2-WI indicate tumor vascularity **(53)**. The tumor frequently can invade the adjacent organs, thereby demonstrating ill-defined, irregular margins. Pleural effusion, ascites, and lymphadenopathy also have been reported (**52**).

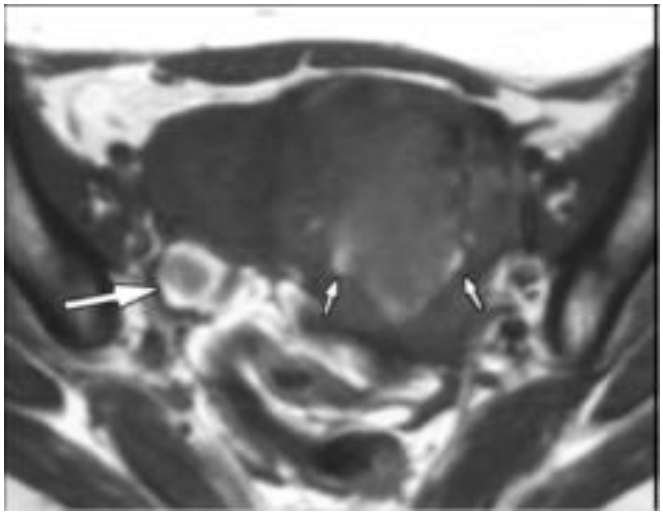

Figure (21): 38-year-old woman who presented with pure primary ovarian choriocarcinoma. A, Axial T1-weighted MR image displays hemorrhage in small cavities (small arrows) at periphery of left adnexal mass and right corpus luteum cyst (large arrow) (**53**).

Findings of Cervical Tumor on MRI:

Cervical tumor on T1W sequences, lesions are usually isointense to the normal cervical tissue and may be invisible. On T2W images, cervical cancer shows a relatively hyperintense signals and is easily differentiated from low-signal-intensity cervical stroma. On dynamic contrast-enhanced MRI, small tumors show homogenous enhancement earlier than the normal stroma of the cervix. Huge tumors are usually show areas of necrosis and may enhance or not but are surrounded by rim of enhancement that make tumor definition easier **(54).**

A critical drawback of staging by MRI is over estimation of parametrial invasion on T2W images in large tumors due to edematous stroma caused by

compression of the tumor or inflammation. This drawback may cause a higher rate of false-positive assessment of invasion of the parametrium in patients with huge tumors, which must be in mind when making the decisions of treatment in these patients **(55)**.

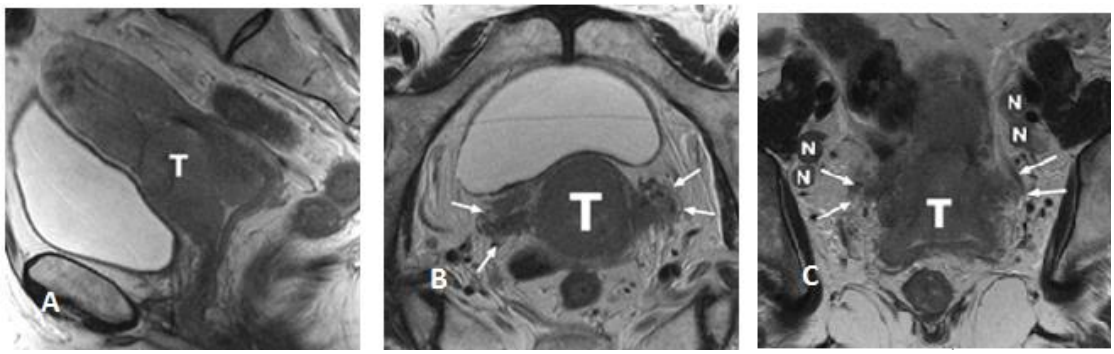

Figure (22): Stage IIB cervical cancer in 42-year-old woman. (A) Sagittal fast spin-echo, (B) axial oblique, and(C) coronal oblique T2-weighted images show cervical cancer (T) involving both anterior and posterior lips of cervix. Tumor invades fibrocervical stroma bilaterally, as shown by loss of low-signal-intensity ring and extends to both parametria (arrows in B). Coronal oblique image shows bilateral parametrial invasion (arrows in C) and enlarged lymph nodes (N in C) **(56).**

MRI findings indicating invasion of the bladder include focal or diffuse interruption of the normal low-signal-intensity posterior bladder wall, nodular or irregularity of the bladder wall, mass bulging into the bladder lumen, or edema. Rectal infiltration is rare and show thickening colonic segments and loss of the wall anteriorly. Prominent strands between the rectal wall and the tumor may also denote rectal invasion **(57).**

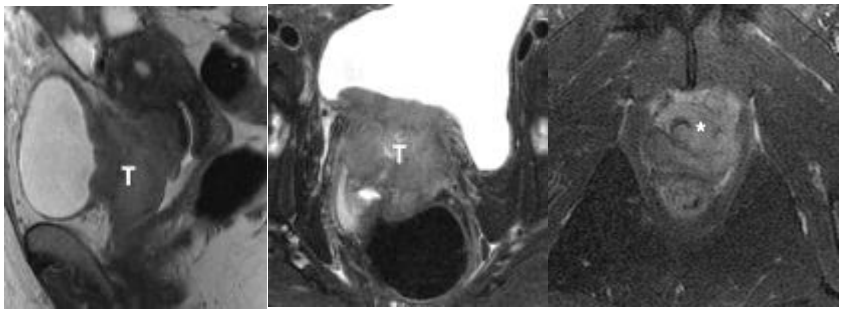

A **B** **C**

Figure (23): Stage IVB cervical cancer in 39-year-old woman. (A) Sagittal fast spin-echo and (B and C) axial fat-suppressed. T2-weighted images show large cervical cancer (T in A and B) involving anterior lip of cervix. Tumor also invades posterior wall of bladder, entire vagina, and urethra (asterisk in C) **(57).**

Vaginal Tumors

MRI finding depending on histological type of malignancy but vaginal cancer in general show signal characteristics in T1w imaging is isointense to the muscle and high signal intensity compared to the muscle in T2w. and the signal intensity in squamous cell carcinoma low signal intensity in T1w and intermediate signal intensity in T2W.**(58)**.

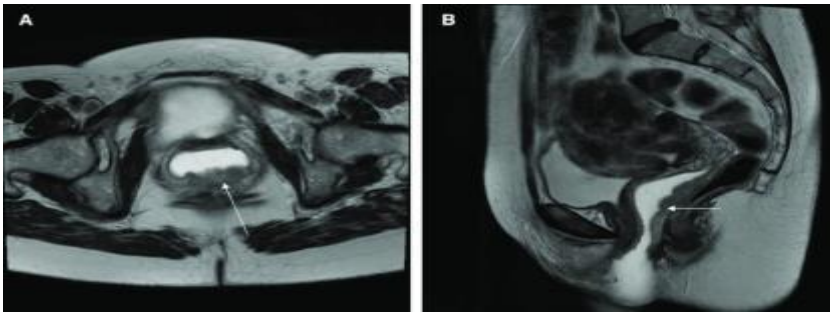

Figure (24): T2 weighted MRI of a patient with vaginal cancer. The lesion shown by the arrow in the posterior wall of the vagina is biopsy-positive vaginal cancer. The lesion involves the entire length of the

posterior vaginal wall up to 0.5 cm from the cervix. There is vaginal water base gel in the vagina which shows up as white and separates the vaginal walls so that the lesion can be seen easier (**58**).

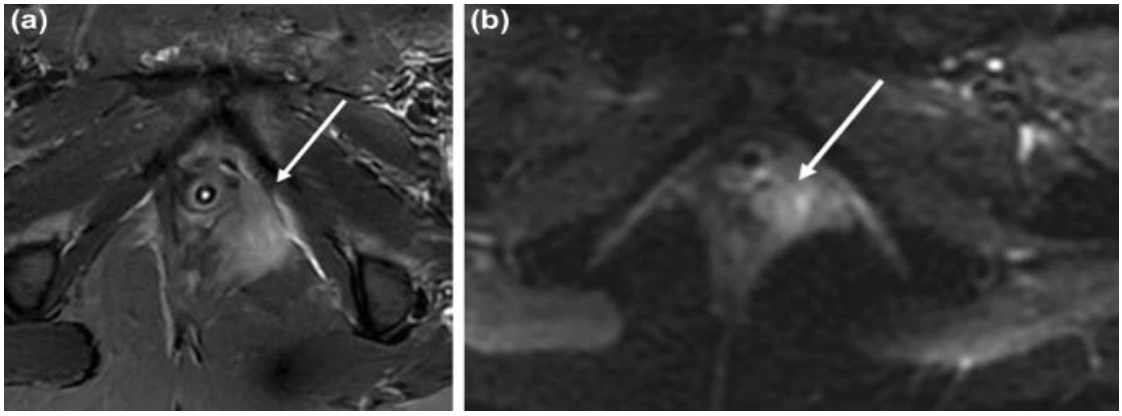

Figure (25): 48-year-old woman with recurrent squamous cell carcinoma of the vagina. **a** Axial T2-weighted fat-saturated MR image shows a hyperintense mass within the left perineum causing mass effect on the left lateral vaginal wall (arrow) and extending into the left periurethral space. **b** DWI shows the lesion (arrow) with restricted diffusion (**59**).

Vulvar Tumors:

MRI useful in assessing size of vulvar lesion and groin lymph node metastasis. The signal characteristic show low to intermediate signal intensity in T1w and intermediate to high signal intensity in T2w with restricted DWI and peripheral enhancement DCE imaging **(60**).

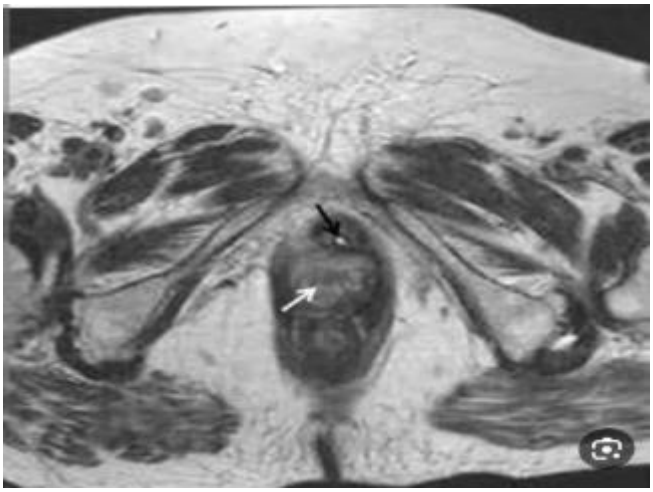

Figure (26): Axial T2-weighted image shows a vulvar mass with heterogeneous intermediate signal intensity. The lesion invades the urethra, which has a urinary catether (black arrow), and the lower third of the vagina (white arrow) **(60).**

References:

1. **Jeong YY, Outwater EK, and Kang HK. (2000):** Imaging evaluation of ovarian masses. *Radiographics*. 20 (5): 1445-1470.
2. **Luczynska E, and Zbigniew K. (2022):** Diagnostic imaging in gynecology. *Ginekologia Polska*. 93(1): 63-69.
3. **Bourgioti C, Konidari M, and Moulopoulos LA. (2023):** Manifestations of Ovarian Cancer in Relation to Other Pelvic Diseases by MRI. *Cancers*. 15(7): 2106
4. **Kishimoto K, Ito K, Awaya H, Matsunaga N, Outwater EK, and Siegelman ES. (2002):** Paraovarian cyst: MR imaging features. *Abdominal Imaging*. 27: 685-689.
5. **Thomassin-Naggara I, Poncelet E, Jalaguier-Coudray A, Guerra A, Fournier LS, and Stojanovic S, et al. (2020):** Ovarian-Adnexal Reporting Data System Magnetic Resonance Imaging (O-RADS MRI) Score for Risk Stratification of Sonographically Indeterminate Adnexal Masses. *JAMA Netw. Open*. 3: e1919896
6. **Thomassin-Naggara I, Aubert E, Rockall A, Jalaguier-Coudray A, Rouzier R, and Daraï E, et al. (2013):** Adnexal Masses: Development

and Preliminary Validation of an MR Imaging Scoring System. *Radiology*. 267: 432–443.

7. **Boger-Megiddo I, and Weiss NS. (2005):** Histologic Subtypes and Laterality of Primary Epithelial Ovarian Tumors. Gynecol. Oncol. 97: 80–83.
8. **Huang J, Chan WC, Ngai CH, Lok V, Zhang L, and Lucero-Prisno,DE, et al. (2022):** Worldwide Burden, Risk Factors, and Temporal Trends of Ovarian Cancer: *A Global Study. Cancers*. 14, 2230.
9. **Folkins AK, and Longacre TA. (2019):** Low-Grade Serous Neoplasia of the Female Genital Tract. *Surg. Pathol. Clin*. 12: 481–513.
10. **Bazot M, Haouy D, Daraï E, Cortez A, Dechoux-Vodovar S, and Thomassin-Naggara I. (2013):** Is MRI a Useful Tool to Distinguish between Serous and Mucinous Borderline Ovarian Tumours? *Clin*. *Radiol*. 68: e1–e8.
11. **Marko J, Marko KI, Pachigolla SL, Crothers BA, Mattu R, and Wolfman DJ. (2019):** Mucinous Neoplasms of the Ovary: Radiologic-Pathologic Correlation. *RadioGraphics*. 39: 982–997.
12. **Peres LC, Cushing-Haugen KL, Köbel M, Harris HR, Berchuck A, and Rossing MA, et al. (2019):** Invasive Epithelial Ovarian Cancer Survival by Histotype and Disease Stage. *JNCI J. Natl. Cancer Inst*. 111: 60–68
13. **Fadare O, and Parkash V. (2019):** Pathology of Endometrioid and Clear Cell Carcinoma of the Ovary. *Surg. Pathol. Clin*. 12: 529–564.
14. **Tanaka YO, Okada S, Yagi T, Satoh T, Oki A, and Tsunoda H, et al. (2010):** MRI of Endometriotic Cysts in Association With Ovarian Carcinoma. *Am. J. Roentgenol*. 194: 355–361.
15. **van Niekerk CC, Bulten J, Vooijs GP, and Verbeek ALM. (2010):** The Association between Primary Endometrioid Carcinoma of the Ovary and Synchronous Malignancy of the Endometrium. *Obstet. Gynecol. Int*. 2010:465162.
16. **Tang YZ, Liyanage S, Narayanan P, Sahdev A, Sohaib A, and Singh N, et al. (2013):** The MRI Features of Histologically Proven Ovarian Cystadenofibromas—An Assessment of the Morphological and Enhancement Patterns. Eur. *Radiol*. 23: 48–56.
17. **Avesani G, Caliolo G, Gui B, Petta F, Panico C, and La Manna V, et al. (2021):** Pearls and Potential Pitfalls for Correct Diagnosis of Ovarian Cystadenofibroma in MRI: A Pictorial Essay. *Korean J. Radiol*. 22: 1809.
18. **Jung DC, Kim SH, and Kim SH. (2006):** MR Imaging Findings of Ovarian ystadenofibroma and Cystadenocarcinofibroma: Clues for the Differential Diagnosis. *Korean J. Radiol*.. 7: 199.
19. **Shinagare AB, Meylaerts LJ, Laury AR, and Mortele KJ. (2012):** MRI Features of Ovarian Fibroma and Fibrothecoma with Histopathologic Correlation. *Am. J. Roentgenol*. 198: W296–W303
20. **Chung BM, bin Park S, Lee JB, Park HJ, Kim YS, and Oh YJ. (2015):** Magnetic Resonance Imaging Features of Ovarian Fibroma, Fibrothecoma, and Thecoma. *Abdom. Imagin*. 40: 1263–1272.
21. **Chen H, Liu Y, Shen L, Jiang M, Yang Z, and Fang G. 2016):** Ovarian Thecoma-Fibroma Groups: Clinical and Sonographic Features with Pathological Comparison. *J. Ovarian Res* 9: 81.
22. **Moon WJ, Koh BH, Kim SK, Kim YS, Rhim HC, and Cho OK, et al. (2000):** Brenner Tumor of the Ovary: CT and MR Findings. *J. Comput. Assist. Tomogr*. 24: 72–76.
23. **Jung SE, Lee JM, Rha SE, Byun JY, Jung JI, and Hahn ST. (2002):** CT and MR imaging of ovarian tumors with emphasis on differential diagnosis. *Radiographics*. 22(6): 1305-1325.
24. **Takeuchi M, Matsuzaki K, Sano N, Furumoto H, and Nishitani H. (2008):** Malignant Brenner Tumor with Transition from Benign to Malignant Components. *J. Comput. Assist. Tomogr*. 32: 553–554.
25. **Euscher ED. (2019):** Germ Cell Tumors of the Female Genital Tract. *Surg*. *Pathol. Clin*.12: 621–649.
26. **Taylor EC, Irshaid L, and Mathur M. (2020):** Multimodality Imaging Approach to Ovarian Neoplasms with Pathologic Correlation. *RadioGraphics*. 41: 289–315.
27. **Elsherif S, Bourne M, Soule E, Lall C, and Bhosale P. (2020):** Multimodality Imaging and Genomics of Granulosa Cell Tumors. *Abdom. Radiol*. 45: 812–827.
28. **Zhang H, Zhang H, Gu S, Zhang Y, Liu X, and Zhang G. (2018):** MR Findings of Primary Ovarian Granulosa Cell Tumor with Focus on the Differentiation with Other Ovarian Sex Cord-Stromal Tumors. J. *Ovarian Res*. 11: 46.
29. **Fotopoulou C, Savvatis K, Braicu E-I, Brink-Spalink V, Darb-Esfahani S, and Lichtenegger W, et al.. (2010):** Adult Granulosa Cell Tumors of the Ovary: Tumor Dissemination Pattern at Primary and Recurrent Situation, Surgical Outcome. *Gynecol. Oncol*. 2010, 119, 285–290.
30. **Slonimsky E, Korach J, Perri T, Davidson T, Apter S, and Inbar Y. (2018):** Gynecological

Lymphoma. *J. Comput. Assist. Tomogr*. 42: 435–440.

31. **Crawshaw J, Sohaib SA, Wotherspoon A, and Shepherd JH. (2007):** Primary Non-Hodgkin's Lymphoma of the Ovaries: Imaging Findings. *Br. J. Radiol*. 80: e155–e158.
32. **Lerwill MF, and Young RH. (2008):** Metastatic Tumors of the Ovary. In Blaustein's Pathology of the Female Genital Tract; Springer: New York, NY, USA. pp. 929–998.
33. **Koyama T, Mikami Y, Saga T, Tamai K, and Togashi K. (2007):** Secondary Ovarian Tumors: Spectrum of CT and MR Features with Pathologic Correlation. *Abdom. Imaging*. 32: 784–795.
34. **Khunamornpong S, Suprasert P, Pojchamarnwiputh S, Na Chiangmai W, Settakorn J, and Siriaunkgul S. (2006):** Primary and Metastatic Mucinous Adenocarcinomas of the Ovary: Evaluation of the Diagnostic Approach Using Tumor Size and Laterality. *Gynecol. Oncol*. 101: 152–157.
35. **Xu Y, Yang J, Zhang Z, and Zhang G. (2015):** MRI for Discriminating Metastatic Ovarian Tumors from Primary Epithelial Ovarian Cancers. *J. Ovarian Res*. 8: 61.
36. **Kurokawa R, Nakai Y, Gonoi W, Mori H, Tsuruga T, and Makise N, et al. (2020):** Differentiation between Ovarian Metastasis from Colorectal Carcinoma and Primary Ovarian Carcinoma: Evaluation of Tumour Markers and "Mille-Feuille Sign" on Computed Tomography/Magnetic Resonance Imaging. *Eur. J. Radiol*. 124: 108823
37. **Wu F, Zhao X, Mi B, Feng LU, Yuan NA, and Lei F,** X**et al. (2015):** Clinical characteristics and prognostic analysis of Krukenberg tumor. *Mol Clin Oncol*. 3:1323–1328
38. **Talerman A. (2002):** Germ Cell Tumors of the Ovary. In Blaustein's Pathology of the Female Genital Tract; Springer: New York, NY, USA. pp. 967–1034.
39. **Saleh M, Bhosale P, Menias CO, Ramalingam P, Jensen C, and Iyer R, et al. (2021):** Ovarian Teratomas: Clinical Features, Imaging Findings and Management. *Abdom. Radiol*. 46: 2293–2307.
40. **Nakayama T, Yoshimitsu K, Irie H, Aibe H, Tajima T, and Nishie A, et al. (2005):** Diffusion-Weighted Echo-Planar MR Imaging and ADC Mapping in the Differential Diagnosis of Ovarian Cystic Masses: Usefulness of Detecting Keratinoid Substances in Mature Cystic Teratomas. *J. Magn. Reson. Imaging*. 22: 271–278.
41. **Outwater EK, Siegelman ES, and Hunt JL. (2001):** Ovarian Teratomas: Tumor Types and Imaging Characteristics. *RadioGraphics*. 21: 475–490.
42. **Yamaoka T, Togashi K, Koyama T, Fujiwara T, Higuchi T, and Iwasa Y, et al. (2003):** Immature Teratoma of the Ovary: Correlation of MR Imaging and Pathologic Findings. *Eur. Radiol*. 13: 313–319.
43. **Northridge JL. (2020):** Adnexal Masses in Adolescents. *Pediatr. Ann*. 49: e183–e187
44. **Laufer M, and Goldstein D. (2005):** Benign and Malignant Ovarian Masses. In Pediatric and Adolescent Gynecology; Lippincott Williams & Wilkins: Philadelphia, PA, USA. p. 685.
45. **Kitajima K, Hayashi M, Kuwata Y, Imanaka K, and Sugimura K. (2003):** MRI Appearances of Ovarian Dysgerminoma. Eur. *J. Radiol. Extra*. 61: **23–25.**
46. **Shaaban AM, Rezvani M, Elsayes KM, Baskin H, Mourad A, and Foster BR, et al. (2014):** Ovarian Malignant Germ Cell Tumors: Cellular Classification and Clinical and Imaging Features. *RadioGraphics*. 3:, 777–801.
47. **Seki H, Takano T, and Sakai K. (2000):** Value of dynamic MR imaging in assessing endometrial carcinoma involvement of the cervix. American *Journal of Roentgenology*. 175(1): 171-176.
48. **Wong FCS, Pang CP, Tang SK, Tung SY, Leung TW, and Sze WK, et a;. (2004):** Treatment results of endometrial carcinoma with positive peritoneal washing, adnexal involvement and serosal involvement. *Clinical Oncology*. 16(5): 350-355.
49. **Manfredi R, Gui B, Maresca G, Fanfani F, and Bonomo L. (2005):** Endometrial cancer: magnetic resonance imaging. *Abdominal Imaging.* 30: 626-636.
50. **Creasman WT. (2005):** Hormone replacement therapy after cancers. *Current Opinion in Oncology*. 17(5): 493-499.
51. **Heller D, and Hricak H. (2000):** Cost-effectiveness of new technologies for staging endometrial cancer. *European Radiology*. 10: S381-5.
52. **Ueno T, Tanaka YO, Nagata M, Tsunoda H, Anno I, and Ishikawa S, et al. (2004):** Spectrum of germ cell tumors: from head to toe. *Radiographics*. 24(2): 387-404.
53. **Balat O, Kutlar I, Ozkur A, Bakir K, Aksoy F, and Ugur MG. (2004):** Primary pure ovarian choriocarcinoma mimicking ectopic pregnancy: a report of fulminant progression. *Tumori Journal*. 90(1): 136-138.
54. **Bipat S, Glas AS, van der Velden J, Zwinderman AH, Bossuyt PM and Stoker J.**

(2003): Computed tomography and magnetic resonance imaging in staging of uterine cervical carcinoma: a systematic review. *Gynecol Oncol*. 91:59 –66.

55. **Scheidler J, and Heuck AF. (2002):** Imaging of cancer of the cervix. *Radiologic Clinics*. 40(3): 577-590.
56. **Hricak H, Gatsonis, C, Chi DS, Amendola MA, Brandt K, and Schwartz LH, et al. (2005):** Role of imaging in pretreatment evaluation of early invasive cervical cancer: results of the intergroup study American College of Radiology Imaging Network 6651–Gynecologic Oncology Group 183. *Journal of Clinical Oncology*. 23(36): 9329-9337.
57. **Jeong YY, Kang HK, Chung TW, Seo JJ, and Park JG. (2003):** Uterine cervical carcinoma after therapy: CT and MR imaging findings. *Radiographics*. 23(4): 969-981.
58. **Anuja J. (2022):** updates in the treatment of vaginal cancer international. *Journal of Gynecologic Caner*. 32:344- 351
59. **Chow L, Tsui BQ, Bahrami S, Masamed R, Memarzadeh S, and Raman SS, et al. (2021):** Gynecologic tumor board: a radiologist's guide to vulvar and vaginal malignancies. *Abdominal Radiology*. 46:5669–5686
60. **Ângela F. (2014)**: Albuquerque, Chantal; Branco, Rui Centro Hospitalar Tondela Viseu, Department of Radiology; Av. Rei D. Duarte . Clinical case Eurorad. ESR. Viseu, Portuga. Pp. 3504-509